

Sulphur and zinc abundances in Galactic stars and damped Ly α systems [★]

P.E. Nissen¹, Y.Q. Chen², M. Asplund³, and M. Pettini⁴

¹ Department of Physics and Astronomy, University of Aarhus, DK-8000 Aarhus C, Denmark. e-mail: pen@ifu.au.dk

² National Astronomical Observatories, Chinese Academy of Sciences, Beijing 100012, P.R. China. e-mail: cyq@bao.ac.cn

³ Research School of Astronomy and Astrophysics, Australian National University, Mount Stromlo Observatory, Cotter Road, Weston, ACT 2611, Australia. e-mail: martin@mso.anu.edu.au

⁴ Institute of Astronomy, University of Cambridge, Madingley Road, Cambridge, CB3 0HA, UK. e-mail: pettini@ast.cam.ac.uk

Received 9 July 2003 / Accepted November 19 2003

Abstract. High resolution spectra of 34 halo population dwarf and subgiant stars have been obtained with VLT/UVES and used to derive sulphur abundances from the $\lambda\lambda 8694.0, 8694.6$ and $\lambda\lambda 9212.9, 9237.5$ S I lines. In addition, iron abundances have been determined from 19 Fe II lines and zinc abundances from the $\lambda\lambda 4722.2, 4810.5$ lines. The abundances are based on a classical 1D, LTE model atmosphere analysis, but effects of 3D hydrodynamical modelling on the [S/Fe], [Zn/Fe] and [S/Zn] ratios are shown to be small. We find that most halo stars with metallicities in the range $-3.2 < [\text{Fe}/\text{H}] < -0.8$ have a near-constant [S/Fe] $\simeq +0.3$; a least square fit to [S/Fe] vs. [Fe/H] shows a slope of only -0.04 ± 0.01 . Among halo stars with $-1.2 < [\text{Fe}/\text{H}] < -0.8$ the majority have [S/Fe] $\simeq +0.3$, but two stars (previously shown to have low α/Fe ratios) have [S/Fe] $\simeq 0.0$. For disk stars with [Fe/H] > -1 , [S/Fe] decreases with increasing [Fe/H]. Hence, sulphur behaves like other typical α -capture elements, Mg, Si and Ca. Zinc, on the other hand, traces iron over three orders of magnitude in [Fe/H], although there is some evidence for a small systematic Zn overabundance ([Zn/Fe] $\simeq +0.1$) among metal-poor disk stars and for halo stars with [Fe/H] < -2.0 . Recent measurements of S and Zn in ten damped Ly α systems (DLAs) with redshifts between 1.9 and 3.4 and zinc abundances in the range $-2.1 < [\text{Zn}/\text{H}] < -0.15$ show an offset relative to the [S/Zn] – [Zn/H] relation in Galactic stars. Possible reasons for this offset are discussed, including low and intermittent star formation rates in DLAs.

Key words. Stars: abundances – Stars: atmospheres – Galaxy: evolution – Galaxies: high-redshift – quasars: absorption lines

1. Introduction

Sulphur is generally regarded as an α -capture element. The work on Galactic stars by François (1987, 1988) supported this view by showing that [S/Fe] increases from zero at solar metallicities to a plateau level of about +0.5 dex in the metallicity range $-1.8 < [\text{Fe}/\text{H}] < -1.0$. This is an analogous behaviour to those of other α -elements, Mg, Si, and Ca – see Norris et al. (2001) and Carretta et al. (2002), who both find $[\alpha/\text{Fe}]$ to be nearly constant at a level of +0.4 dex in the metallicity range $-4 < [\text{Fe}/\text{H}] < -1$ and then to decrease towards the solar $[\alpha/\text{Fe}]$ ratio for [Fe/H] > -1 . The standard interpretation is that this

trend arises from the time delay in the production of about two thirds of the iron by supernovae (SNe) of Type Ia relative to the near-instantaneous release of the α -elements by Type II SNe. In this connection it should be noted that the metallicity at which Type Ia SNe start to contribute (the “knee” of the $[\alpha/\text{Fe}]$ – [Fe/H] trend) seems to depend on the orbital properties of the stars. Halo stars with [Fe/H] ~ -1 belonging to the outer halo tend to have lower $[\alpha/\text{Fe}]$ than stars in the inner halo (Nissen & Schuster 1997; Stephens & Boesgaard 2002; Gratton et al. 2003). Stephens & Boesgaard find a slope of -0.15 for the mean $[\alpha/\text{Fe}]$ vs. [Fe/H] for 53 stars in the metallicity range $-3.8 < [\text{Fe}/\text{H}] < -0.6$, but this is for a sample with special kinematics, i.e. stars with large maximum distances from the Galactic center and/or the Galactic plane or stars having extreme retrograde motion.

Send offprint requests to: P.E. Nissen

[★] Based on observations collected at the European Southern Observatory, Chile (ESO No. 67.D-0106)

Recent observations of the $\lambda\lambda 8694.0, 8694.6$ Å S I lines in spectra of metal-poor stars by Israelian & Rebolo (2001) have, however, challenged the view that sulphur is an α -element. Their data, obtained with the 4-m William Herschel Telescope on La Palma, suggest that $[S/Fe]$ increases linearly with decreasing $[Fe/H]$ to a level as high as $[S/Fe] \sim +0.7$ at $[Fe/H] = -2.0$. The study of Takada-Hidai et al. (2002), based on Keck High Resolution Echelle Spectrograph (HIRES) observations, supports a quasi linear dependence of $[S/Fe]$ on $[Fe/H]$ although in their case $[S/Fe]$ reaches only +0.5 dex at $[Fe/H] = -2.0$.

As a possible explanation of the high value of $[S/Fe]$ in metal-poor stars, Israelian & Rebolo (2001) proposed that very massive supernovae with exploding He-cores and a high explosion energy make a significant contribution to the early chemical evolution of galaxies. According to Nakamura et al. (2001) these hypernovae overproduce S with respect to O, Mg and Fe. With this intriguing possibility in mind a more thorough investigation of sulphur abundances in halo stars seems worthwhile.

A clarification of the trend of S abundances is also much needed in deciphering the chemical enrichment of damped Ly α systems (DLAs), widely regarded as the progenitors of present-day galaxies at high redshift. The importance of sulphur stems from the fact that, unlike most other heavy elements, S is not depleted onto dust. Consequently, observations of the relatively weak S II triplet resonance lines at $\lambda\lambda 1250, 1253, 1259$ Å yield a direct measurement of the abundance of S in DLAs. Another element for which this is the case is Zn, and indeed most of our current knowledge of the chemical evolution of the universe at high redshift is based on surveys of $[Zn/H]$ in DLAs (e.g. Pettini et al. 1999; Prochaska & Wolfe 2002). If S is an α -capture element, then its abundance relative to Zn (assumed to be an iron-peak element) could be used as ‘a chemical clock’ to date the star-formation process at high z . Specifically, if a major star formation episode in a DLA occurred within ≈ 0.5 Gyr prior to the time when we observe the galaxy, we would expect to measure an enhanced $[S/Zn]$ ratio, and *vice versa*. Measurements of $[S/Zn]$ in DLAs have been relatively scarce until recently, but are now becoming available in increasing numbers thanks the Ultraviolet and Visual Echelle Spectrograph (UVES) on the ESO Very Large Telescope (VLT). The VLT/UVES combination affords high spectral resolution and high efficiency over most of the optical spectrum, from blue and near-UV wavelengths to the far red. However, without a secure knowledge of the behaviour of S in metal-poor Galactic stars we clearly stand little chance of interpreting the situation at high z .

In the present paper we report on a survey of sulphur abundances in 34 metal-poor dwarf stars based on high resolution observations of the $\lambda\lambda 8694.0, 8694.6$ and $\lambda\lambda 9212.9, 9237.5$ Å S I lines obtained with UVES. The $\lambda\lambda 4722.2, 4810.5$ Å Zn I lines are also included in our spectra, allowing us to study the Galactic evolution of both sulphur and zinc.

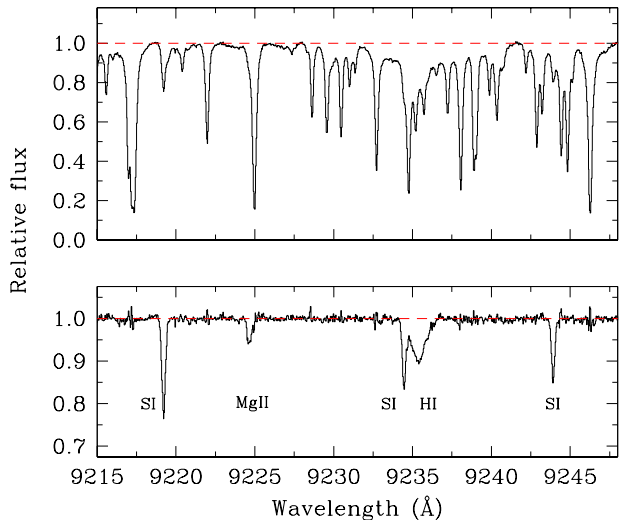


Fig. 1. Portion of the VLT/UVES spectrum of HD 110621 ($V = 9.9$, $[Fe/H] = -1.66$) in the far red. Top panel: the spectrum before removal of the numerous telluric H₂O lines which occur in this region. Bottom panel: the spectrum after division by that of the B-type star HR 5488 using the IRAF task `telluric`. The S I triplet, a Mg II line and the Paschen ζ H I line of HD 110621 can all be clearly seen. Note that the spectrum shown has not been corrected for the radial velocity of the star (which introduces a shift of +6.4 Å), and that the wings of the H I line have been removed by the continuum fitting. Excessive noise in the stellar spectrum is seen where strong H₂O lines have been removed.

2. Observations and data reduction

2.1. UVES observations

Previous determinations of sulphur abundances in metal-poor stars, including those by Israelian & Rebolo (2001) and Takada-Hidai et al. (2002), have been based on the high excitation ($\chi_{\text{exc}} = 7.87$ eV) $\lambda\lambda 8694.0, 8694.6$ S I lines. However, these lines are very weak in metal-poor dwarfs and giants (with equivalent widths $W < 3$ mÅ at $[Fe/H] \sim -2.0$), and become vanishingly small at $[Fe/H] \sim -2.5$. In our survey we have taken advantage of the high efficiency in the far red of the VLT/UVES instrument (Dekker et al. 2000) and concentrated on the stronger S I triplet ($\chi_{\text{exc}} = 6.52$ eV) at $\lambda\lambda 9212.9, 9228.1, 9237.5$ Å. The dichroic mode of UVES was used to cover the spectral region 6700 – 10000 Å in the red arm and 3750 – 5000 Å in the blue arm; the latter region includes a number of Fe II lines suitable for determining the iron abundance, as well as the Zn I lines at 4722.2 and 4810.5 Å.

The observations were carried out using the UVES image slicer #1 (Dekker et al. 2002) which has an entrance aperture of 2.1×2.7 arcsec and makes 3 slices along the 0.7 arcsec wide entrance slit with a total length of 8.0 arcsec.

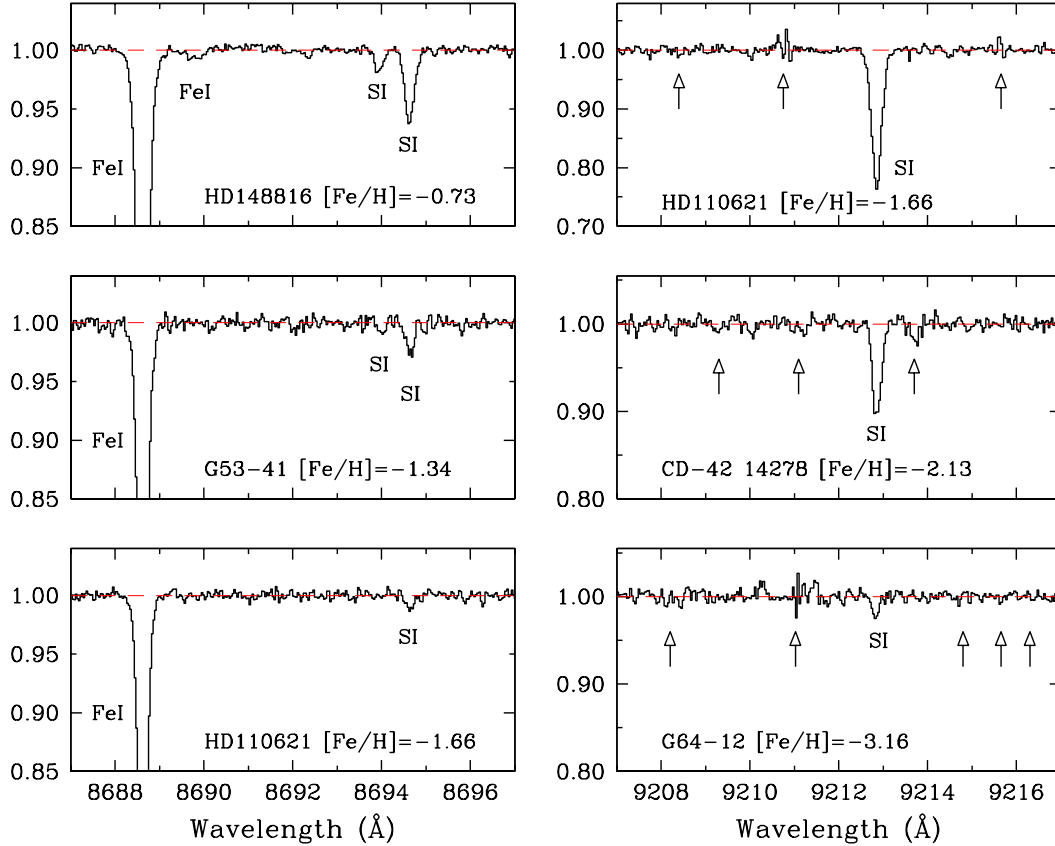


Fig. 2. Left: A sequence of spectra around the $\lambda\lambda 8694.0, 8694.6$ Si I lines. Right: A sequence of spectra around the $\lambda 9212.9$ Si I line. The arrows indicate wavelengths where telluric H₂O lines have been removed.

The resulting resolution of the spectra is $\lambda/\Delta\lambda \simeq 60\,000$ with 4 pixels per spectral resolution element.

Program stars were selected from the Strömgren photometric catalogue of Schuster & Nissen (1988) supplemented with a few very metal-poor stars from Ryan et al. (1999). The selection criteria were: $5700 < T_{\text{eff}} < 6500$ K, $3.7 < \log g < 4.4$ and a smooth distribution of metallicities from $[\text{Fe}/\text{H}] = -3.2$ to -0.6 . The UVES spectra were obtained in service mode during the period March – June, 2001. The total integration time for a $V = 11$ mag star was about 60 min, split into three separate exposures so that cosmic ray hits could be removed by comparison of the three spectra. The sky background could be checked adjacent to the stellar spectrum, but was insignificant (except for emission lines) even for the faintest star (G64-12, $V = 11.46$). Typical S/N ratios are 300 in the blue spectral region, 250–300 at the $\lambda\lambda 8694.0, 8694.6$ Si I lines, and 150–200 in the region of the $\lambda\lambda 9212.9, 9228.1, 9237.5$ Si I triplet.

2.2. Reduction of the spectra

The blue spectra were reduced with standard MIDAS routines for order definition, background subtraction, flat-field correction, order extraction and wavelength calibra-

tion. Bias, dark current and scattered light corrections are included in the background subtraction. The spectra were then normalized by a continuum function determined by fitting a spline curve to a set of pre-selected continuum windows estimated from the solar atlas. Finally, correction for the radial velocity of the star, measured from 20–30 narrow lines, was applied before the measurement of equivalent widths. For a few stars, it was checked that reduction with NOAO’s IRAF echelle package gave nearly identical results.

The red spectra were reduced in the same way as the blue spectra but using the IRAF echelle package. A problem with the $9212\text{--}9238$ Å region is the presence of numerous, strong telluric H₂O lines, see Fig. 1. To remove these lines, fast rotating, early-type stars were observed on each night and reduced in the same way as the program stars. The IRAF task `telluric` was then applied to remove the telluric lines. When the early-type star is observed at about the same airmass as the program star this technique also serves to remove a residual fringing of a few percent in the red region ($\lambda > 7000$ Å) remaining after the flatfielding of the spectra.

A sequence of spectra of stars spanning the whole metallicity range of the sample is shown in Fig. 2. As

seen, the S I line at 9212.9 Å can be clearly detected in a $[\text{Fe}/\text{H}] \sim -3.2$ star.

2.3. Equivalent widths

Equivalent widths of the Fe II, Zn I and S I lines were measured by Gaussian fitting, or direct integration if the fit was poor. For the present set of data, we could estimate empirically the accuracy of our equivalent widths by comparing two independent sets of measurements for nine stars (HD 103723, HD 104004, HD 110621, HD 121004, HD 140283, HD 146296, G 16-13, G 66-30, and G 64-12) which were observed twice (on different nights). The first set of observations was carried out on March 9 and 10 while the second set was made from March 12 to May 9, 2001. The total exposure time for each star was the same at each epoch. The comparison of the Fe II and Zn I lines is shown in Fig. 3. As can be seen from the figure, the data fall close to the 1:1 line with a standard deviation of only $\pm 0.84 \text{ m}\text{\AA}$. This corresponds to an error of $\pm 0.6 \text{ m}\text{\AA}$ for one measurement of an equivalent width in the blue part of the UVES spectra.

The weak S I lines at 8694.0 and 8694.6 Å could be measured in the more metal-rich part of our sample ($[\text{Fe}/\text{H}] > -1.5$). Among the stronger triplet lines $\lambda 9228.1$ falls very close to the center of the Paschen ζ H I line and its equivalent width could therefore not be measured in a reliable way. The other two S I lines are, however, ideal for abundance determination in the metallicity range $-3 < [\text{Fe}/\text{H}] < -1$.

The comparison of equivalent widths of S I lines measured from spectra obtained on different nights is shown in Fig. 4. Again, the data are evenly distributed around the 1:1 line, but with a larger scatter for the $\lambda\lambda 9212.9, 9237.5$ lines ($\sigma = \pm 3.3 \text{ m}\text{\AA}$) than is the case for the $\lambda\lambda 8694.0, 8694.6$ pair ($\sigma = \pm 0.8 \text{ m}\text{\AA}$). The reason is the lower S/N in the 9212 – 9238 Å region, made worse by the telluric lines. Thus, the equivalent widths of the $\lambda\lambda 9212.9, 9237.5$ lines have been measured with a precision of $\pm 2.3 \text{ m}\text{\AA}$ (one spectrum), whereas the precision for the weaker $\lambda\lambda 8694.0, 8694$ pair is as good as $\pm 0.6 \text{ m}\text{\AA}$.

The error of the measurement of the equivalent widths of the $\lambda\lambda 9212.9, 9237.5$ S I lines is particular important for estimating the precision of the sulphur abundance determinations for the most metal-poor stars, where the lines are weak. An independent check of the estimated error may be obtained by comparing the sulphur abundances derived from the $\lambda 9212.9$ and the $\lambda 9237.5$ S I line, respectively. For nine stars with $[\text{Fe}/\text{H}] < -2$ having equivalent widths of the S I lines ranging from 5 to 36 mÅ the mean difference of the sulphur abundances derived from the two sets of lines is 0.03 dex with a rms scatter of the difference of ± 0.08 dex, only. This is, in fact, a smaller dispersion than expected from the estimated equivalent error of $\pm 2.3 \text{ m}\text{\AA}$, which should then be considered as a conservative estimate.

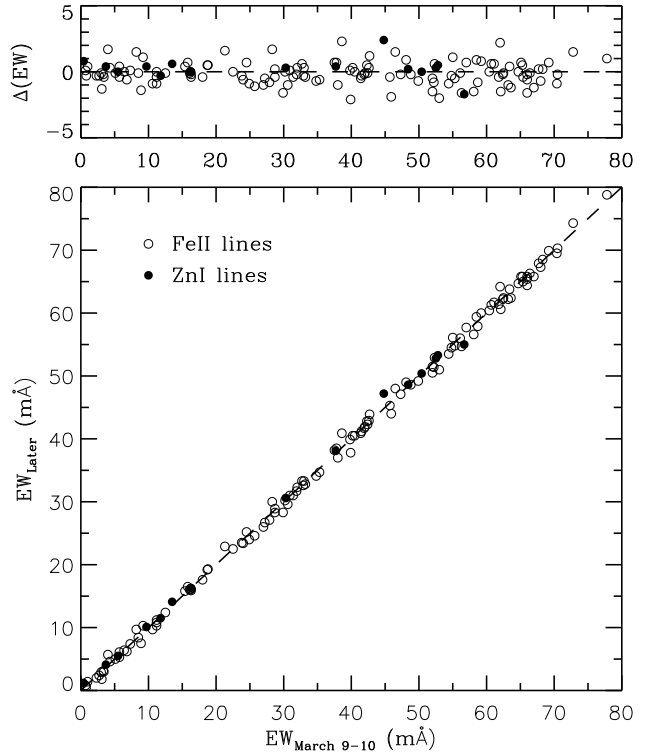


Fig. 3. A comparison of equivalent widths of Fe II and Zn I lines measured from two sets of spectra for nine stars observed on March 9 – 10 and March 12 – May 9, 2001, respectively.

The measured equivalent widths for 19 Fe II lines, the two Zn I lines and the four S I lines in 34 program stars are listed in Table A1¹. When no value is given it is either because the line is too strong or too weak to provide a reliable abundance, or, in the case of the $\lambda\lambda 9212.9, 9237.5$ S I lines, is affected by residuals from the removal of strong telluric H₂O lines. In addition to the stars listed in Table A1, three stars, HD 99382, BD –13 3834 and G 18-54, were observed, but they turned out to be double-lined spectroscopic binaries, and are excluded from our abundance analysis.

3. Stellar parameters

The determinations of stellar parameters follows the method described by Nissen et al. (2002). Here we briefly outline the procedure and discuss the precision of T_{eff} , $\log g$ and $[\text{Fe}/\text{H}]$. The final values of T_{eff} and $\log g$ are given in Table 3 together with values for $[\text{Fe}/\text{H}]$ and the microturbulence as derived from Fe II lines (Sect. 4.1). As the calibrations of T_{eff} and $\log g$ depend somewhat on $[\text{Fe}/\text{H}]$, the determination of the parameters is an iterative process.

¹ Table A1 is only available in electronic form at the CDS via anonymous ftp to cdsarc.u-strasbg.fr (130.79.128.5) or via <http://cdsweb.u-strasbg.fr/cgi-bin/qcat?J/A+A/.../...>

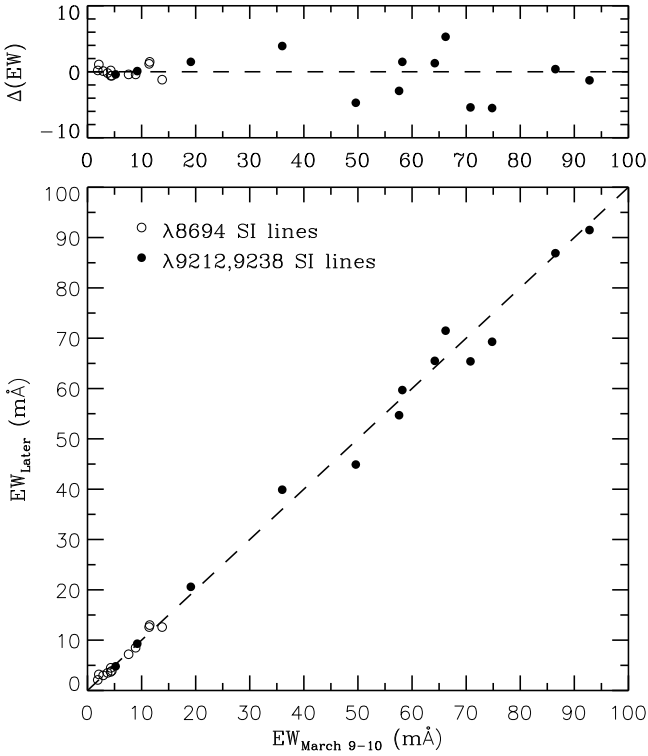


Fig. 4. A comparison of equivalent widths of the $\lambda\lambda 8694.0, 8694.6$ and $\lambda\lambda 9212.9, 9237.5$ Å SI lines measured from two sets of spectra for nine stars.

3.1. Effective temperature

T_{eff} was determined from the $b - y$ and $V - K$ colour indices using the IRFM calibrations of Alonso et al. (1996) as modified by Nissen et al. (2002). The Strömgren $wby-\beta$ photometry was taken from Schuster & Nissen (1988) for the large majority of the stars supplemented with unpublished photometry of Schuster et al. (2003) for the remaining stars. The $(b - y)_0$ calibration of Schuster & Nissen (1989) including a zero-point correction of $+0.005$ mag (Nissen 1994) was used to derive the interstellar reddening excess. If $E(b - y) > 0.015$, the reddening is considered significant and the V magnitude as well as the m_1 and the c_1 indices are corrected according to the relations given by Nissen et al. (2002). These values and the reddening estimates are given in Table 1.

The K photometry was taken from Carney (1983), Alonso et al. (1994) and the Two Micron All Sky Survey (2MASS)². In this connection we note that the 2MASS K

magnitudes are on the so-called K -short system (Cutri et al. 2003), whereas those of Carney (1983) are on the CIT (California Institute of Technology) system and Alonso et al.'s (1994) magnitudes are on the TCS (Telescope Carlos Sánchez) system. Small differences between these systems may exist. Carpenter (2001) has derived an average transformation $K(2\text{MASS}) = K(\text{CIT}) - 0.024$ without any colour term. For our actual sample of metal-poor turnoff and subgiant stars the agreement is even better. Twelve stars with both CIT and 2MASS photometry have a mean difference in K of 0.002 only with a rms-dispersion of the difference of 0.026. For 16 stars with both Alonso et al. and 2MASS photometry the mean K difference (TCS - 2MASS) is -0.019 with a dispersion of 0.030. Hence, the three systems agree within ± 0.02 mag in K for our sample, which according to the Alonso et al. (1996) T_{eff} calibration of $V - K$ corresponds to an error of ± 20 K in T_{eff} . The corresponding effect on the derived abundances is small compared to other error sources as seen from Table 4. We have, therefore, adopted the straight mean of the K magnitudes if two or three sources were available. Table 1 lists the corresponding $V - K$ value corrected for interstellar reddening according to the relation $E(V - K) = 2.7E(B - V) = 3.8E(b - y)$ (Savage & Mathis 1979), if $E(b - y) > 0.015$.

Comparing the T_{eff} values determined from $b - y$ and $V - K$ we find a mean difference ($\Delta = T_{\text{eff}}(b - y) - T_{\text{eff}}(V - K)$) $\langle \Delta \rangle = +44$ K for 25 stars with a standard deviation of $\sigma(\Delta) = 78$ K (one star). Similar values were found for the sample of metal-poor stars in Nissen et al. (2002). The mean value of $T_{\text{eff}}(b - y)$ and $T_{\text{eff}}(V - K)$ is adopted for the 25 stars. For nine stars without K photometry, a value $T_{\text{eff}}(b - y) - 22$ K has been adopted. The typical observational errors are 0.007 mag in $b - y$ and 0.05 mag in $V - K$, which correspond to an error of ± 50 K in T_{eff} in either case. Taking into account the uncertainty in the reddening estimate (also corresponding to about ± 50 K in T_{eff}), we estimate the $1-\sigma$ statistical error of T_{eff} to be around 70 K.

3.2. Surface gravity

The surface gravity was determined from the fundamental relation

$$\log \frac{g}{g_{\odot}} = \log \frac{\mathcal{M}}{\mathcal{M}_{\odot}} + 4 \log \frac{T_{\text{eff}}}{T_{\text{eff},\odot}} + 0.4(M_{\text{bol}} - M_{\text{bol},\odot}) \quad (1)$$

where \mathcal{M} is the mass of the star and M_{bol} the absolute bolometric magnitude.

The absolute visual magnitude M_V was determined from a new calibration of the Strömgren indices derived by Schuster et al. (2003) on the basis of Hipparcos parallaxes, and also directly from the Hipparcos parallax (ESA 1997) if available with an error $\sigma(\pi)/\pi < 0.3$. Column 12 and 13 of Table 1 list the photometric and the parallax based values of M_V . They compare reasonably well for the 18 stars having $M_{V,\text{par}}$. Excluding one star, G 186-26, with a large

² This publication makes use of data products from the Two Micron All Sky Survey, which is a joint project of the University of Massachusetts and the Infrared Processing and Analysis Center/California Institute of Technology, funded by NASA and the National Science Foundation. K magnitudes were taken from the Second Incremental Release. Additional values from the recent full release have only a marginal effect on the derived T_{eff} and abundances.

Table 1. Strömgren photometry, colour excess, $V - K$ index, T_{eff} from $b - y$ and $V - K$, spectroscopic value of $[\text{Fe}/\text{H}]$, and absolute magnitudes derived from the Strömgren photometry and from the Hipparcos parallax including an error corresponding to the parallax error. If $E(b - y) > 0.015$, the V magnitudes and the photometric indices have been corrected for interstellar absorption.

Star	V_0	$(b - y)_0$	m_0	c_0	β	E_{b-y}	$(V - K)_0$	$T_{e,b-y}$ [K]	$T_{e,V-K}$ [K]	$[\text{Fe}/\text{H}]$	$M_{V,\text{phot}}$	$M_{V,\text{par}}$	$\pm\sigma$
BD-13°3442	10.153	0.277	0.059	0.379	2.622	0.031	1.129	6526	6475	-2.61	4.03		
CD-30°18140	9.859	0.302	0.053	0.340	2.606	0.021	1.214	6285	6259	-1.88	3.93	4.18	0.46
CD-35°14849	10.568	0.321	0.040	0.293	2.603	0.010		6147		-2.41	4.24		
CD-42°14278	10.216	0.361	0.040	0.229	2.576	0.009		5834		-2.12	4.83		
HD 103723	9.947	0.329	0.104	0.306	2.625	0.027		6064		-0.82	4.37	4.36	0.46
HD 105004	10.194	0.360	0.124	0.261	2.616	0.027	1.337	5830	6007	-0.86	4.78		
HD 106038	10.179	0.342	0.092	0.264	2.583	-0.018	1.408	5940	5898	-1.42	4.69	4.99	0.36
HD 108177	9.671	0.330	0.059	0.287	2.594	-0.001	1.342	6047	6033	-1.74	4.36	4.87	0.26
HD 110621	9.906	0.337	0.067	0.324	2.595	0.008		6011		-1.66	3.75	4.15	0.46
HD 121004	9.031	0.395	0.140	0.268	2.588	0.012		5617		-0.77	4.89	5.15	0.18
HD 140283	7.213	0.380	0.033	0.284	2.564	0.015	1.580	5734	5646	-2.42	3.53	3.42	0.12
HD 146296	9.761	0.383	0.143	0.268	2.581	-0.004		5693		-0.74	4.87	4.27	0.38
HD 148816	7.287	0.366	0.117	0.312	2.582	-0.005	1.448	5822	5824	-0.73	4.20	4.22	0.08
HD 160617	8.733	0.347	0.051	0.331	2.584	0.011	1.408	5953	5909	-1.79	3.27	3.42	0.31
HD 179626	9.210	0.373	0.095	0.293	2.588	0.015	1.560	5750	5649	-1.14	4.24	3.59	0.39
HD 181743	9.687	0.351	0.052	0.224	2.582	0.000		5885		-1.93	4.97	4.95	0.34
HD 188031	10.148	0.328	0.058	0.310	2.592	-0.001		6076		-1.79	4.02		
HD 193901	8.660	0.383	0.099	0.221	2.568	-0.002	1.533	5652	5691	-1.12	5.16	5.46	0.12
HD 194598	8.354	0.344	0.091	0.269	2.588	-0.011		5928		-1.17	4.63	4.62	0.15
HD 215801	10.044	0.334	0.049	0.330	2.572	-0.018	1.402	6071	5940	-2.29	3.47		
LP 815-43	10.774	0.272	0.054	0.376	2.623	0.032	1.117	6558	6508	-2.67	4.17		
G 011-044	11.091	0.335	0.061	0.248	2.588	-0.009	1.381	6023	5967	-2.09	4.80		
G 013-009	9.916	0.292	0.054	0.369	2.609	0.019	1.195	6402	6319	-2.27	3.68		
G 016-013	9.951	0.387	0.129	0.286	2.583	0.008	1.627	5676	5529	-0.76	4.60		
G 018-039	10.392	0.346	0.073	0.286	2.581	-0.007	1.412	5926	5894	-1.52	4.32		
G 020-008	9.948	0.356	0.047	0.251	2.574	0.001	1.465	5879	5831	-2.28	4.58	4.56	0.43
G 024-003	10.393	0.346	0.062	0.268	2.585	0.017	1.414	5925	5894	-1.67	4.51		
G 029-023	10.230	0.339	0.059	0.332	2.590	0.008	1.400	6010	5923	-1.80	3.49		
G 053-041	11.022	0.356	0.083	0.271	2.589	0.004	1.460	5848	5810	-1.34	4.54		
G 064-012	11.330	0.282	0.046	0.330	2.622	0.030	1.114	6458	6563	-3.17	4.54		
G 064-037	11.144	0.299	0.057	0.329	2.626	0.009	1.235	6328	6308	-3.12	4.21		
G 066-030	10.950	0.287	0.077	0.354	2.634	0.018	1.177	6381	6311	-1.52	4.25		
G 126-062	9.478	0.330	0.063	0.327	2.588	-0.004	1.455	6060	5825	-1.64	3.75	4.11	0.37
G 186-026	10.829	0.306	0.041	0.339	2.608	0.011	1.229	6280	6266	-2.62	3.73	5.20	0.50

difference but also with the largest uncertainty of $M_{V,\text{par}}$, the mean difference ($\Delta = M_{V,\text{phot}} - M_{V,\text{par}}$) is $\langle \Delta \rangle = -0.07$ mag with a standard deviation of $\sigma(\Delta) = 0.32$ mag. The corresponding error in M_V is ± 0.22 mag. This induces an error of about ± 0.1 dex in $\log g$. Taking into account possible errors in the bolometric correction (adopted from Alonso et al. (1995)) and the mass as derived by interpolating in the $M_V - \log T_{\text{eff}}$ diagram between the α -element enhanced evolutionary tracks of VandenBerg et al. (2000), we estimate that the error of $\log g$ is about ± 0.15 dex.

4. Abundances

The determination of abundances is based on α -element enhanced ($[\alpha/\text{Fe}] = +0.4$, $\alpha = \text{O, Ne, Mg, Si, S, Ca, and Ti}$) 1D model atmospheres with T_{eff} , $\log g$ and $[\text{Fe}/\text{H}]$ values as given in Table 3 and a microturbulence of 1.5 km s^{-1} .

The models were computed with the MARCS code using updated continuous opacities (Asplund et al. 1997) and including UV line blanketing by millions of absorption lines. LTE is assumed both in constructing the models and in deriving abundances.

The Uppsala abundance analysis program, EQWIDTH, was used to calculate theoretical equivalent widths from the models. An elemental abundance is determined by requiring that the calculated equivalent width should match the observed one. When more than one line of the same species were measured for a star, the mean value is adopted by giving equal weight to each line.

4.1. Iron

By inspecting the blue spectra, 19 apparently unblended Fe II lines were selected for determining the iron abundance. Differential $\log gf$ values of these lines were derived by an inverted abundance analysis of four ‘standard’ stars, HD 103723, HD 160617, G 13-09 and HD 140283 adopting iron abundances of $[\text{Fe}/\text{H}] = -0.79, -1.79, -2.30$ and -2.42 , respectively, from Nissen et al. (2002). In this calculation, only lines with equivalent widths between 5 and 50 mÅ were included. If a differential $\log gf$ value is available for more than one of the four standard stars, then the mean value (given in Table 2) is adopted. We note that the $[\text{Fe}/\text{H}]$ values of Nissen et al. (2002) are based on very weak Fe II lines in the red spectral region measured from extremely high S/N spectra and analyzed differentially to the solar flux spectrum. The same procedure could not be applied to the blue Fe II lines because they are quite strong in the solar spectrum and often blended with weak lines making the solar equivalent width measurement difficult.

In calculating abundances from the Fe II lines we adopted the Unsöld (1955) approximation to the Van der Waals interaction constant with an enhancement factor $E_\gamma = 2.5$. But the adopted value of E_γ does not have a large effect on $[\text{Fe}/\text{H}]$ since most Fe II lines in the stars are weak, especially in metal-poor stars. For the most metal-rich stars in our sample the change of $[\text{Fe}/\text{H}]$ is around $+0.03$ dex when E_γ is changed from 2.5 to 1.5.

In the more metal-poor stars ($[\text{Fe}/\text{H}] < -1.5$) the Fe II lines are so weak that the derived metallicity is practically independent of the microturbulence. For such stars we have assumed $\xi_{\text{micro}} = 1.5 \text{ km s}^{-1}$. For the more metal-rich stars ξ_{micro} has been determined by requesting that the derived $[\text{Fe}/\text{H}]$ values should be independent of equivalent width. The error of ξ_{micro} is about $\pm 0.2 \text{ km s}^{-1}$.

The present sample has 10 stars in common with the sample of Nissen et al. (2002). The metallicities of these stars range from $[\text{Fe}/\text{H}] = -0.75$ to -2.70 . The mean difference (present – 2002) is $< \Delta[\text{Fe}/\text{H}] > = -0.01$ with a standard deviation of ± 0.04 dex. This small scatter shows that precise $[\text{Fe}/\text{H}]$ values have been determined in both papers.

4.2. Sulphur

The $\log gf$ values of the S I lines listed in Table 2 are adopted from the Coulomb approximation calculations of Lambert & Luck (1978). From the equivalent widths of the $\lambda\lambda 8694.0, 8694.6$ S I lines in the solar flux spectrum (Kurucz et. al. 1984) of 11.0 and 28.8 mÅ, respectively, we derive a solar sulphur abundance of $\log \epsilon(\text{S}) = 7.20$. This is also the meteoritic abundance (Grevesse & Sauval 1998), but given possible errors in the $\log gf$ values (the NIST database lists values that are 0.04 dex higher than those of Lambert & Luck) the exact agreement is quite fortuitous. Anyhow, when deriving the differential sulphur abundance with respect to the Sun, i.e. $[\text{S}/\text{H}]$, a possible error in $\log gf$ is of no concern. Furthermore, since the

Table 2. The list of lines used to determine the abundances of Fe, S and Zn. Measured equivalent widths are given for three representative stars: (a) HD 194598, $[\text{Fe}/\text{H}] = -1.17$, (b) HD 160617, $[\text{Fe}/\text{H}] = -1.79$, and (c) HD 140283, $[\text{Fe}/\text{H}] = -2.42$.

ID	Wavelength Å	Exc. Pot. eV	$\log gf$	$W(\text{a})$ mÅ	$W(\text{b})$ mÅ	$W(\text{c})$ mÅ
Fe II	4128.74	2.58	-3.73	15.0	5.0	
Fe II	4178.86	2.58	-2.61	55.8	39.7	17.8
Fe II	4233.16	2.58	-2.01	81.3	68.1	41.8
Fe II	4416.83	2.78	-2.65	46.3	29.5	11.2
Fe II	4489.18	2.83	-2.96	32.5	17.3	5.5
Fe II	4491.41	2.85	-2.80	37.9	21.4	7.4
Fe II	4508.29	2.85	-2.41	55.1	37.4	16.2
Fe II	4515.34	2.84	-2.56	48.9	31.2	12.4
Fe II	4520.23	2.81	-2.66	46.0	28.9	11.0
Fe II	4522.63	2.84	-2.22	64.6	48.3	22.5
Fe II	4541.52	2.85	-3.04	28.4	14.4	4.5
Fe II	4555.89	2.83	-2.43	53.9	37.5	16.1
Fe II	4576.34	2.84	-3.01	28.5	15.0	5.0
Fe II	4582.83	2.84	-3.24	20.9	9.8	3.2
Fe II	4583.83	2.81	-1.91	82.1	63.8	37.9
Fe II	4620.52	2.83	-3.36	17.5	7.4	2.5
Fe II	4656.98	2.89	-3.66	8.1	3.1	
Fe II	4666.75	2.83	-3.31	17.9	7.5	2.9
Fe II	4923.93	2.89	-1.45		82.9	58.5
Zn I	4722.16	4.03	-0.39	23.8	8.6	3.9
Zn I	4810.54	4.08	-0.17	29.0	13.5	5.5
S I	8693.96	7.87	-0.56	1.9		
S I	8694.64	7.87	0.03	5.1	4.1	
S I	9212.87	6.52	0.38	77.0	57.4	19.8
S I	9237.54	6.52	0.01	53.2	34.4	9.2

$\lambda\lambda 8694.0, 8694.6$ S I lines are quite weak and apparently without any blends in the solar spectrum, the derived $[\text{S}/\text{H}]$ is not subject to the kind of systematic errors which may affect $[\text{Zn}/\text{H}]$ as discussed in Sect 4.3.

The flux around the $\lambda 9237.5$ S I line is slightly depressed relative to the true continuum by the broad wing of the Paschen ζ H I line at 9229 Å. In this connection, we note that the equivalent widths of the S I lines were measured relative to the local, apparent continuum around the lines. Furthermore, when deriving the sulphur abundance we neglected the contribution of the H I line to the line absorption coefficient. For a few representative stars a spectrum synthesis of the region around the $\lambda 9237.5$ S I line was carried out including the line absorption contribution from the Paschen ζ H I line calculated as described by Seaton (1990). This exercise shows that the correction to the sulphur abundance derived from the equivalent width of the $\lambda 9237.5$ S I line is at most about $+0.07$ dex for our hottest stars and decreases with decreasing T_{eff} . In the case of the $\lambda 9212.9$ S I line, which is further away from the H I line, the corresponding correction is negligible. An empirical confirmation of the effect is seen in Fig. 5, where the difference of sulphur abundances derived from the $\lambda 9212.9$ and $\lambda 9237.5$ lines is plotted as a function of T_{eff} . Given

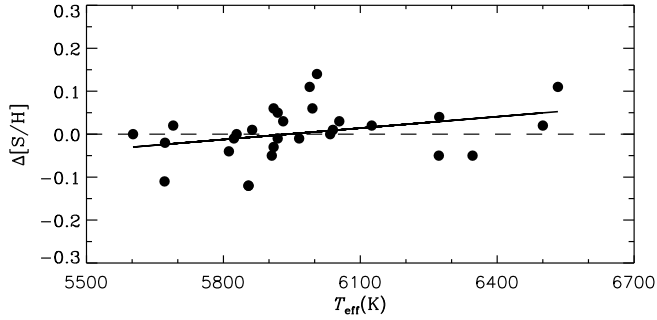


Fig. 5. The difference in S abundances derived from the $\lambda 9212.9$ and $\lambda 9237.5$ S I lines. The least squares fit to the data is shown. The rms deviation between the two sets of abundances is ± 0.06 dex.

the small size of the effect and the uncertainty in the line broadening theory of this high-series Paschen H I line, we have not included any correction for the H I line absorption. In this connection, we note that for the two most metal-poor stars in our sample, G 64-12 and G 64-37, only the $\lambda 9212.9$ S I line could be detected and used for deriving the S abundance.

The $\lambda\lambda 9212.9, 9237.5$ S I lines are too strong in the solar spectrum and the spectral region is too crowded with telluric H₂O lines to allow a reliable solar S abundance to be determined from these lines. In order to check that this pair provides S abundances on the same scale as the $\lambda\lambda 8694.0, 8694.6$ lines, we make use of the fact that for 18 of the 34 program stars the S abundance has been derived from both the $\lambda\lambda 8694.0, 8694.6$ and the $\lambda\lambda 9212.9, 9237.5$ pairs. The mean abundance difference is 0.03 dex and the standard deviation is ± 0.08 dex. Hence, we are confident that the two sets of S I lines provide [S/H] values on the same scale.

4.3. Zinc

The zinc abundance is based on two Zn I lines at 4722.2 and 4810.5 Å. The $\log gf$ values (-0.39 and -0.17 respectively) were adopted from the calculations of Biémont & Godefroid (1980). From equivalent widths measured in the solar flux spectrum (Kurucz et. al. 1984) of 70.3 and 78.3 mÅ, respectively, and using a solar model atmosphere computed with the same code as that for the stars, we derive a solar zinc abundance of $\log \epsilon(\text{Zn}) = 4.57$. This is 0.10 dex lower than the meteoritic abundance of 4.67 ± 0.04 (Grevesse & Sauval 1998). The same problem was encountered by Biémont & Godefroid (1980), who derived a solar photospheric zinc abundance of $\log \epsilon(\text{Zn}) = 4.60$ from six Zn I lines (including $\lambda 4722.2$ and $\lambda 4810.5$) using the Holweger-Müller (1974) model of the Sun. This difference between photospheric and meteoritic Zn abundances may well be due to a systematic error in the $\log gf$ values of the Zn I lines. However, by determining differential Zn abundances with respect to the Sun, i.e. [Zn/H], using our solar photospheric abundance of $\log \epsilon(\text{Zn}) = 4.57$ as a reference, errors in $\log gf$ will cancel. On the other hand, it should be

Table 3. The derived values of the effective temperature, surface gravity, microturbulence, and the abundances of iron, sulphur and zinc.

Star	T_{eff} [K]	$\log g$ [cgs]	ξ_{turb} [km/s]	[Fe/H]	[S/H]	[Zn/H]
BD-13°3442	6500	4.16	1.5	-2.61	-2.31	
CD-30°18140	6272	4.13	1.5	-1.88	-1.63	-1.82
CD-35°14849	6125	4.11	1.5	-2.41	-2.10	-2.27
CD-42°14278	5812	4.25	1.5	-2.12	-1.82	-2.04
HD 103723	6040	4.26	1.3	-0.82	-0.84	-0.95
HD 105004	5919	4.36	1.2	-0.86	-0.85	-0.86
HD 106038	5919	4.30	1.2	-1.42	-1.00	-1.25
HD 108177	6034	4.25	1.5	-1.74	-1.39	-1.65
HD 110621	5989	3.99	1.5	-1.66	-1.34	-1.63
HD 121004	5595	4.31	1.0	-0.77	-0.43	-0.58
HD 140283	5690	3.69	1.5	-2.42	-2.11	-2.35
HD 146296	5671	4.17	1.2	-0.74	-0.54	-0.69
HD 148816	5823	4.14	1.2	-0.73	-0.49	-0.61
HD 160617	5931	3.77	1.5	-1.79	-1.40	-1.81
HD 179626	5699	3.92	1.2	-1.14	-0.85	-1.14
HD 181743	5863	4.32	1.5	-1.93	-1.59	-1.94
HD 188031	6054	4.03	1.5	-1.79	-1.47	-1.76
HD 193901	5672	4.38	1.0	-1.12	-0.95	-1.18
HD 194598	5906	4.25	1.3	-1.17	-0.99	-1.22
HD 215801	6005	3.81	1.5	-2.29	-2.01	-2.21
LP 815-43	6533	4.25	1.5	-2.67	-2.43	
G 011-044	5995	4.29	1.5	-2.09	-1.71	-1.90
G 013-009	6360	4.01	1.5	-2.27	-1.81	-2.20
G 016-013	5602	4.17	1.0	-0.76	-0.47	-0.81
G 018-039	5910	4.09	1.5	-1.52	-1.15	-1.44
G 020-008	5855	4.16	1.5	-2.28	-1.85	-2.15
G 024-003	5910	4.16	1.5	-1.67	-1.29	-1.61
G 029-023	5966	3.82	1.5	-1.80	-1.50	-1.83
G 053-041	5829	4.15	1.3	-1.34	-1.05	-1.29
G 064-012	6511	4.39	1.5	-3.17	-2.81	
G 064-037	6318	4.16	1.5	-3.12	-2.78	
G 066-030	6346	4.24	1.5	-1.52	-1.28	-1.52
G 126-062	5943	3.97	1.5	-1.64	-1.31	-1.71
G 186-026	6273	4.25	1.5	-2.62	-2.43	

noted that the Zn I lines in the solar spectrum are quite strong and hence subject to errors in the adopted solar flux microturbulence (1.15 km s^{-1}) and the Van der Waals damping constant (an enhancement factor $E_{\gamma} = 1.5$ relative to the Unsöld approximation was adopted). The solar equivalent widths of the Zn I $\lambda\lambda 4722.2, 4810.5$ lines are also quite uncertain due to blends in their wings. Hence, the scale of the [Zn/H] values for our metal-poor stars could be in error by up to 0.10 dex.

4.4. Results

The abundances [Fe/H], [S/H] and [Zn/H] derived for the stars in our sample are listed in Table 3 together with the stellar atmospheric parameters. For the most metal-poor stars the Zn I lines are too weak ($W < 2 \text{ mÅ}$) to provide reliable Zn abundances, and the value of [Zn/H] is not given.

In Fig. 6, $[S/Fe]$ is plotted as a function of $[Fe/H]$. All our program stars have space velocities that are typical of halo stars, and are shown with filled circles. In addition, we have plotted disk stars from Chen et al. (2002), who determined sulphur abundances from five weak Si I lines including the $\lambda\lambda 8694.0, 8694.6$ pair.

Fig. 7 shows $[Zn/Fe]$ vs. $[Fe/H]$. Here the data for the disk stars are from Chen et al. (2003), who observed the weak Zn I line ($\chi_{\text{exc}} = 5.79 \text{ eV}$) at 6362.35 \AA and determined $[Zn/H]$ by a differential model atmosphere analysis with respect to the Sun. This Zn line lays in the midst of a very broad and weak Ca I auto-ionization line (Mitchell & Mohler 1965), but its equivalent width can still be measured reliably with respect to the local continuum. In the solar flux spectrum (Kurucz et al. 1984) its equivalent width is close to 22.0 m\AA and the line appears unblended. Hence this line is highly suitable for determining Zn abundances in disk stars. The $\lambda 6362.35$ line is not covered by the UVES spectra of the present program, but in the very high S/N spectra of Nissen et al. (2002) we were able to detect the line for three of the more metal-rich halo stars and to derive $[Zn/H]$ in a differential analysis with respect to the Sun: HD 103723, $W = 4.9 \text{ m\AA}$, $[Zn/H] = -0.85$; HD 106038, $W = 2.6 \text{ m\AA}$, $[Zn/H] = -1.18$; and HD 121004, $W = 9.5 \text{ m\AA}$, $[Zn/H] = -0.53$. These Zn abundances compare reasonably well with those given in Table 3 (the differences being ≤ 0.1 dex), indicating that the values of $[Zn/H]$ derived in the halo stars from the Zn I $\lambda\lambda 4722.2, 4810.5$ lines are approximately on the same scale as $[Zn/H]$ for the disk stars.

Finally, Fig. 8 shows $[S/Zn]$ vs. $[Zn/H]$. Here the disk stars are those from Chen et al. (2002, 2003) for which both S and Zn abundances are available.

4.5. Statistical abundance errors

The main contributions to the random errors in the abundances arise from the errors in the equivalent width measurements and the uncertainties in the model atmosphere parameters. The level of the latter contribution has been estimated by changing T_{eff} of the stellar models by 100 K, $\log g$ by 0.2 dex and the metallicity by 0.2 dex. Table 4 shows the corresponding changes in the various abundance ratios. Evidently, $\Delta T_{\text{eff}} = 100 \text{ K}$ has a negligible effect of $[Fe/H]$, and rather small effects on the other abundance ratios, except $[S/Zn]$. $[Fe/H]$ and $[S/H]$ are quite sensitive to $\log g$ but the $\log g$ effects nearly cancel in the S/Fe ratio. We also see that the effect of changing the metal content of the model atmosphere is negligible. Finally, we note that the possible error in the microturbulence parameter only has a significant effect on the derived abundances for the more metal-rich stars.

Errors in the measured equivalent widths were discussed in Sect. 2.3 and found to be about $\pm 0.6 \text{ m\AA}$ for the Fe II and the Zn I lines as well as the $\lambda\lambda 8694.0, 8694.6$ Si I pair, whereas the error for the $\lambda\lambda 9212.9, 9237.5 \text{ \AA}$ Si I lines is $\pm 2.3 \text{ m\AA}$. Adopting these errors, and taking into

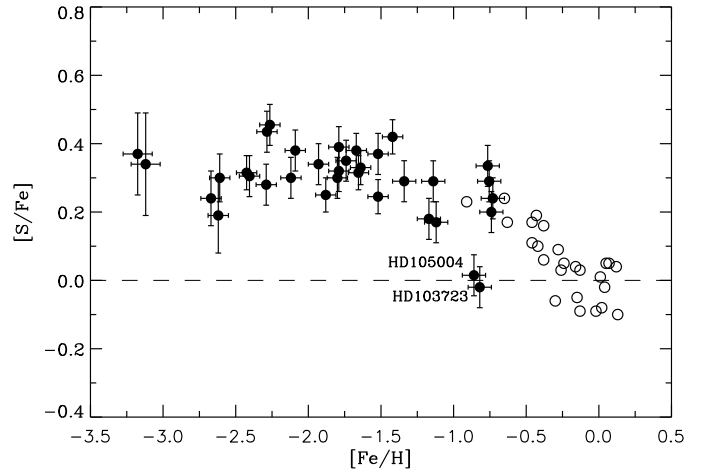


Fig. 6. $[S/Fe]$ vs. $[Fe/H]$. Filled circles refer to halo stars from the present program. Open circles are disk stars with abundances from Chen et al. (2002). The error bars indicate $1\text{-}\sigma$ statistical errors of $[S/Fe]$ and $[Fe/H]$.

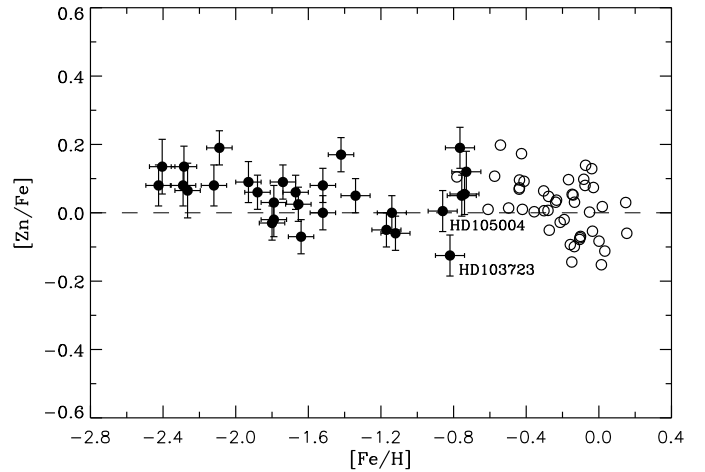


Fig. 7. $[Zn/Fe]$ vs. $[Fe/H]$. Filled circles: halo stars; open circles: disk stars from Chen et al. (2003). The error bars indicate $1\text{-}\sigma$ statistical errors of $[Zn/Fe]$ and $[Fe/H]$.

account the number of lines observed for a given star and the contribution from the estimated errors in T_{eff} ($\pm 70 \text{ K}$), $\log g$ (± 0.15 dex) and ξ_{turb} ($\pm 0.2 \text{ km s}^{-1}$), we have estimated individual abundance errors for each star. These errors are indicated with 1-sigma error bars in Figs. 6, 7, and 8. At the lowest metallicities the dominating error contribution comes from the measurement of the equivalent widths of the weak absorption lines, whereas errors in the atmospheric parameters give the largest contribution for the more metal-rich stars.

4.6. Systematic abundance errors

In this section we discuss systematic abundance errors arising from the modelling of the line formation processes using plane parallel, homogeneous model atmospheres and the assumption of LTE.

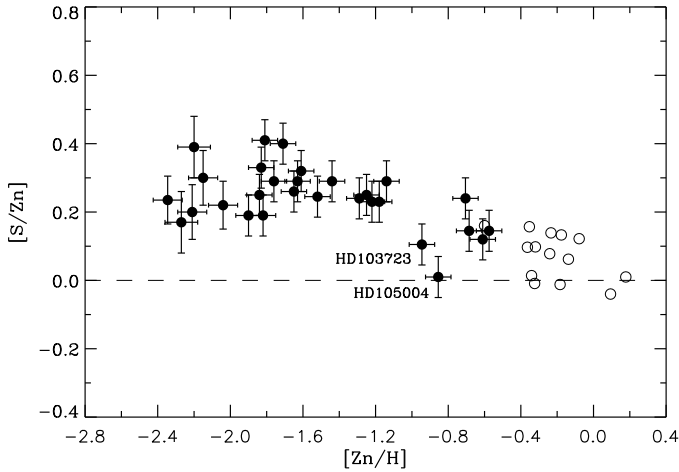


Fig. 8. [S/Zn] vs. [Zn/H]. Filled circles: halo stars; open circles: disk stars from Chen et al. (2002, 2003). The error bars indicate 1- σ statistical errors of [S/Zn] and [Fe/H].

Table 4. Changes in derived abundances resulting from the listed changes in model atmosphere parameters.

	$\Delta[\frac{\text{Fe}}{\text{H}}]$	$\Delta[\frac{\text{S}}{\text{H}}]$	$\Delta[\frac{\text{Zn}}{\text{H}}]$	$\Delta[\frac{\text{S}}{\text{Fe}}]$	$\Delta[\frac{\text{Zn}}{\text{Fe}}]$	$\Delta[\frac{\text{S}}{\text{Zn}}]$
$\Delta T_{\text{eff}} = 100 \text{ K}$	0.01	-0.04	0.04	-0.05	0.03	-0.08
$\Delta \log g = 0.2$	0.07	0.06	0.03	-0.01	-0.04	0.03
$\Delta[\text{Fe}/\text{H}] = 0.2$	0.01	0.01	0.01	0.00	0.00	0.00
$\Delta \xi_{\text{turb}} = 0.3 \text{ km/s}^{\text{a}}$	-0.06	-0.02	-0.02	0.04	0.04	0.00

^a The abundance changes caused by changing ξ_{turb} by 0.3 km s^{-1} are maximum values valid for the more metal-rich stars.

4.6.1. The influence of stellar granulation

Much attention has recently been paid to the effect on abundance determinations of three-dimensional (3D) hydrodynamical modelling of convection and granulation in stellar atmospheres. As first shown by Asplund et al. (1999), there is a very significant surface cooling in metal-poor stars caused by the near adiabatic cooling of rising and expanding elements coupled with the lack of radiative heating due to the low line opacity. The effect on lines formed in the upper atmosphere can be very large. As an example, Asplund & García Pérez (2001) estimated 3D effects on oxygen abundances derived from OH lines to be of the order of -0.6 dex for turnoff stars with $[\text{Fe}/\text{H}] < -2.0$.

To investigate the 3D effects on the sulphur and zinc lines used in the present study a differential study similar to that described by Asplund & García Pérez (2001) has been carried out. The results are given in Table 5 for two sets of model atmospheres with metallicities of $[\text{Fe}/\text{H}] = 0.0, -1.0, -2.0$ and -3.0 . The first set has T_{eff} and $\log g$ close to the solar values, whereas the second set represents stars close to the turnoff of the halo population. For each 3D model atmosphere, the S and Zn abundances are those reproducing the equivalent widths computed with 1D MARCS with identical stellar parameters and spectral line data; for Fe, the results are culled

from the identical calculations presented by Asplund & García Pérez (2001) and correspond to the average of six Fe II lines. The spectrum syntheses assume $[\text{S}/\text{Fe}] = +0.4$ and $[\text{Zn}/\text{Fe}] = 0.0$ for $[\text{Fe}/\text{H}] \leq -1$, but the results are almost identical for reasonable $[\text{S}/\text{Fe}]$ and $[\text{Zn}/\text{Fe}]$. It can be seen that the maximum 3D effect occurs for the most metal-poor stars: the 3D abundance is higher than the 1D value by 0.07 to 0.13 dex in the case of the $\lambda\lambda 9212.9, 9237.5$ S I lines. Interestingly, however, there is a similar 3D effect on the Fe abundance derived from Fe II lines. Hence, it appears that we are in the favourable situation that the S/Fe ratio is quite immune to 1D – 3D effects, with net differences of $\Delta[\text{S}/\text{Fe}] \lesssim 0.05$ dex for the stellar parameters typical of our sample. Similarly, the 3D effects on the Zn/Fe ratio are very small ($\Delta[\text{Zn}/\text{Fe}] \lesssim 0.05$ dex). The small 3D effects and the fact that they in general have the same sign are a consequence of the similarity in line formation depths of these S I, Zn I and Fe II lines.

4.6.2. Non-LTE effects

The S and Fe abundances have been derived from lines belonging to the main ionization stages of the elements, i.e. the neutral stage for S and the first ionized stage for Fe. Furthermore, the lines correspond to high excitation levels and are weak in our stars. Hence, they are formed deep in the stellar atmospheres where only small departures from LTE are expected. This has been confirmed in the case of the Fe II lines by Thévenin & Idiart (1999). According to Takada-Hidai et al. (2002) non-LTE effects on the weak, high excitation S I lines at 8694 \AA are estimated to be small (< 0.05 dex). The good agreement found in Sect 4.2 between sulphur abundances derived from the $\lambda\lambda 8694.0, 8694.6$ pair and the $\lambda\lambda 9212.9, 9237.5$ lines suggests that non-LTE effects on the 9212–9238 S I triplet are also small.

The case of zinc is more difficult. With an ionization potential, $\chi_{\text{ion}}(\text{Zn I}) = 9.39 \text{ eV}$, there are approximately equal numbers of neutral and ionized zinc atoms at the temperatures and electron pressures of the line forming regions in the atmospheres of our stars. Hence, an over-ionization of Zn I relative to LTE, as is the case for Fe I (Thévenin & Idiart 1999), would lead to an underestimate of the abundance of Zn in the LTE analysis of Zn I lines. However, such an over-ionization effect on Zn I is likely to be smaller than the equivalent effect for Fe I, since $N_{\text{Zn I}} \sim N_{\text{Zn II}}$ whereas $N_{\text{Fe I}} \ll N_{\text{Fe II}}$. Furthermore, there may be departures from LTE in the excitation balance of Zn I, since the lower level from which the lines originate is the first excited level of Zn I. The discrepancy noted above between the meteoritic Zn abundance $\log \epsilon(\text{Zn}) = 4.67$ and the photospheric value of 4.57 may be due to such non-LTE problems. Given the complex structure of the Zn atom, a thorough study of non-LTE effects on the determination of Zn abundances is clearly needed but, to our knowledge, none has been carried out yet. Here we simply

Table 5. The effects of 3D hydrodynamical model atmospheres on the derived sulphur, zinc and iron abundances relative to those estimated with classical 1D models ($\Delta(\log\epsilon) = \log\epsilon(3D) - \log\epsilon(1D)$). Both the 1D and 3D abundances have been computed assuming LTE. It should be noted that the S I 9212.9 Å and S I 9237.5 Å lines are very strong ($W > 100 \text{ mÅ}$) at $[\text{Fe}/\text{H}] = 0.0$ and hence are sensitive to the spectral line broadening. Similarly, the S I 8694.6 Å line is very weak ($W < 0.5 \text{ mÅ}$) at $[\text{Fe}/\text{H}] = -3.0$.

T_{eff} [K]	$\log g$	[Fe/H]	$\Delta(\log\epsilon) = \log\epsilon(3D) - \log\epsilon(1D)$					
			S I 8694.6 Å	S I 9212.9 Å	S I 9237.5 Å	Zn I 4722.2 Å	Zn I 4810.5 Å	Fe II
5767	4.44	-0.0	-0.04	-0.01	-0.01	+0.02	+0.02	-0.02
5822	4.44	-1.0	+0.02	+0.02	+0.02	+0.01	+0.00	+0.04
5837	4.44	-2.0	+0.06	+0.13	+0.11	+0.09	+0.09	+0.10
5890	4.44	-3.0	+0.05	+0.08	+0.08	+0.08	+0.08	+0.09
6191	4.04	-0.0	+0.03	+0.11	+0.09	-0.08	-0.06	-0.01
6180	4.04	-1.0	+0.04	+0.01	+0.03	-0.02	-0.03	+0.02
6178	4.04	-2.0	+0.04	+0.09	+0.09	+0.03	+0.03	+0.06
6205	4.04	-3.0	+0.04	+0.08	+0.07	+0.04	+0.04	+0.07

note that, by analyzing our Zn I lines relative to the solar flux spectrum, the problem is somewhat reduced.

Ideally, the non-LTE calculations should be done in combination with 3D models. This is, however, a very demanding task, which has only recently become feasible (e.g. Kiselman & Nordlund 1995; Kiselman 1997; Uitenbroek 1998; Asplund et al. 2003). For complex atoms like Zn, the computationally less demanding 1.5D non-LTE problem³ would be a good starting point, as recently attempted for Fe I (Shchukina & Bueno 2001). It is noteworthy that the 3D non-LTE results can be significantly different from both the 1D non-LTE and the 3D LTE results. There are, however, very good reasons why quite small ($\lesssim 0.1$ dex) 3D non-LTE corrections are expected in the case of S I. The S I lines are formed in deep atmospheric layers where the differences between 1D and 3D model atmospheres are small. One therefore expects similar non-LTE abundance corrections in 1D and 3D, as for example appears to be the case for O I.

5. Discussion

5.1. Sulphur as an α -capture element

As can be seen from Fig. 6, the halo stars are distributed around $[\text{S}/\text{Fe}] \simeq +0.3$ except for two deviating stars, HD 103723 and HD 105004, that are known to have solar-like $[\alpha/\text{Fe}]$ ratios as discussed in the next paragraph. Using

³ The approximation of treating an ensemble of vertical atmospheric columns extracted from a 3D model as separate plane-parallel 1D model atmospheres on which the 1D non-LTE line formation calculations are performed before averaging, is normally referred to as a 1.5D non-LTE calculation. Such a procedure ignores all horizontal radiative transfer in the 3D model atmosphere. While the results are not quantitatively exact, they can nevertheless provide a qualitative assessment of the general behaviour of the full 3D non-LTE problem and yield a useful estimate of the 3D non-LTE effects.

a maximum likelihood program that takes into account individual errors in both x and y, we obtain a fit for the halo stars (excluding HD 103723 and HD 105004)

$$[\text{S}/\text{Fe}] = 0.240 (\pm 0.024) - 0.042 (\pm 0.014) \cdot [\text{Fe}/\text{H}]$$

with a reduced chi-square $\chi_{red}^2 = 1.28$. If HD 103723 and HD 105004 are included the relation becomes

$$[\text{S}/\text{Fe}] = 0.153 (\pm 0.023) - 0.085 (\pm 0.013) \cdot [\text{Fe}/\text{H}],$$

but then χ_{red}^2 increases to an unacceptable high value of 2.3. In any case the slope is much smaller than the corresponding slope of the fit to the disk star data:

$$[\text{S}/\text{Fe}] = -0.014 (\pm 0.015) - 0.308 (\pm 0.040) \cdot [\text{Fe}/\text{H}].$$

Hence, there is no tendency in our halo star data for a continuing strong linear rise of $[\text{S}/\text{Fe}]$ with decreasing $[\text{Fe}/\text{H}]$, as claimed by Israelian & Rebolo (2001). At $[\text{Fe}/\text{H}] = -2$ their data suggest $[\text{S}/\text{Fe}] \simeq +0.7$, whereas our relation corresponds to $[\text{S}/\text{Fe}] = +0.32$. We note in this connection that their sample includes only three stars with $[\text{Fe}/\text{H}] < -1.8$ and none below $[\text{Fe}/\text{H}] = -2.3$, whereas our sample includes 14 stars in the range $-3.2 < [\text{Fe}/\text{H}] < -1.8$ and seven below $[\text{Fe}/\text{H}] = -2.3$. Furthermore, the error bars on their sulphur abundance determinations are large due to the weakness of the S I 8694.6 Å line; in our study we circumvent this problem with the 9212.9 and 9237.5 Å lines which are well suited for sulphur abundance determinations below $[\text{Fe}/\text{H}] = -2$. Hence, our conclusion is that there is no need to invoke element production by hypernovae or very massive supernovae to explain the general behaviour of sulphur. Our data are in good agreement with traditional Galactic evolution models with near-instantaneous production of α -elements by Type II supernovae and delayed production of the iron-peak elements (e.g. Chiappini et al. 1999, Goswami & Prantzos 2000).

All stars from the present investigation (plotted with filled circles) have halo kinematics, including six stars with $-0.9 < [\text{Fe}/\text{H}] < -0.7$ which have Galactic rotational velocities of less than 50 km s^{-1} i.e. well below the characteristic rotational velocity of thin disk stars (225 km s^{-1}) and thick disk stars (175 km s^{-1}). As shown by Nissen & Schuster (1997), there is an overlap between halo and thick disk stars in the metallicity range $-1.0 < [\text{Fe}/\text{H}] < -0.6$. Four of our six stars in this metallicity range have enhanced S/Fe ratios like the thick disk stars, but two (HD 103723 and HD 105004) have a solar S/Fe ratio. These two stars also show solar α /Fe ratios in other α -elements, such as O, Mg, Si, Ca, and Ti (Nissen & Schuster 1997). On the basis of the stars' Galactic orbits, Nissen & Schuster suggested that they may have been accreted from dwarf galaxies with a chemical evolution that has proceeded more slowly than in the inner part of our Galaxy, where the 'normal' halo stars formed. The fact that S and the classical α -elements, Mg, Si and Ca, exhibit the same behaviour in these 'anomalous' stars is a further indication that sulphur belongs to this group of elements. Thus, there seems to be little ground, on the basis of our data, for the reservations expressed by Prochaska et al. (2000) concerning the use of S as an α -element in the analysis of abundance ratios in DLAs.

5.2. Zinc as a tracer of iron

Zinc is an interesting element with a number of possible nucleosynthesis channels: neutron capture (*s*-processing) in low and intermediate mass stars as well as explosive burning in Type II and Ia SN (Matteucci et al. 1993). Furthermore, zinc is a key element in studies of elemental abundances of damped Ly α systems, because it is one of the few elements which in the interstellar medium are not depleted onto dust and measurements of its interstellar absorption lines have several other practical advantages (Pettini, Boksenberg & Hunstead 1990).

Interstellar iron, on the other hand, can exhibit large gas depletions, and it has thus become customary to use Zn as a tracer of Fe in studies aimed at investigating the chemical evolution and dust content of galaxies, particularly at high redshifts. The underlying assumption is that the abundances of Zn and Fe vary in lockstep, as originally found by Sneden, Gratton, & Crocker (1991) although their data, obtained with 2-3 m class telescopes, exhibited considerable scatter.

Our ignorance of the nucleosynthetic origin of Zn has prompted some to question the validity of using it as a proxy for Fe. We can now reassess the validity of this assumption with modern data such as those presented here. Inspection of Fig. 7 shows that, within the errors, $[\text{Zn}/\text{Fe}]$ is indeed approximately solar, at least between $[\text{Fe}/\text{H}] = 0$ and -2 . Over this range the mean of the 61 measurements shown in Fig. 7 is $[\text{Zn}/\text{Fe}] = +0.03 \pm 0.08$ (1σ). A similar conclusion was recently reached by Mishenina et al. (2002) who published a survey of Zn abundances in

90 disk and halo stars based on the equivalent widths of the $\lambda\lambda 4722.2, 4810.5, 6362.35$ Zn I lines in high resolution spectra of dwarf and giant stars and concluded that their data "confirm the well-known fact that the ratio $[\text{Zn}/\text{Fe}]$ is almost solar at all metallicities".

Looking more closely at the data in Fig. 7, there may be hints of subtle trends which, if confirmed by larger samples, could provide clues to the nucleosynthetic origin of Zn. For example, Prochaska et al. (2000) claimed that in thick disk stars $[\text{Zn}/\text{Fe}] \simeq +0.1$. This mild overabundance of Zn relative to Fe in thick disk stars is also present in the Mishenina et al. (2002) sample, once the stars are separated on the basis of their kinematics into halo, thick and thin disk populations, as recently pointed out by Nissen (2003). Furthermore, there seems to be a gradient in $[\text{Zn}/\text{Fe}]$ as a function of $[\text{Fe}/\text{H}]$ for the halo stars in the Mishenina et al. sample with the highest values of $[\text{Zn}/\text{Fe}]$ being measured in the most metal-poor stars. The few stars in the present study with $[\text{Fe}/\text{H}] < -2.0$ show a similar effect, with a mean $[\text{Zn}/\text{Fe}] \simeq +0.1$ (see Fig. 7). On the other hand, before making too much of these trends, it is important to bear in mind that there may well be systematic errors at the ± 0.10 dex level in the determinations of $[\text{Zn}/\text{Fe}]$, as discussed in Sect. 4.3. Clearly, $[\text{Zn}/\text{Fe}]$ in halo and disk stars should be studied further, both observationally and in terms of Galactic chemical evolution models.

Notwithstanding these uncertainties, it can be seen from Fig. 8 that the $[\text{S}/\text{Zn}]$ ratio shows the same trend vs. metallicity as the classical $[\alpha/\text{Fe}]$ trend, i.e. a plateau at $[\text{S}/\text{Zn}] \simeq +0.25$ until $[\text{Zn}/\text{H}] \simeq -1.0$ and then a decline of $[\text{S}/\text{Zn}]$ to the solar ratio at $[\text{Zn}/\text{H}] \simeq 0$. Complications may arise, however, in the transition region between the halo and the disk where the 'low'- α stars identified to date occur. More measurements in this metallicity regime would be highly desirable.

5.3. Sulphur and zinc in damped Ly α systems

Armed with the results of Fig. 8, we are now in a position to examine the $[\text{S}/\text{Zn}]$ ratio in DLAs and compare it to the values measured in Galactic stars. Despite the large database of abundance measurements in DLAs accumulated over the last few years, there are still relatively few determinations of $[\text{S}/\text{Zn}]$ in DLAs. The reasons are two-fold. First, the rest wavelengths of the S II triplet $\lambda\lambda 1250, 1253, 1259$ are so close to the wavelength of Ly α (1215.67 \AA) that the S II lines often fall within the Ly α forest, where blending can be a problem. Second, with rest wavelengths $\lambda\lambda 2026, 2062$, the Zn II doublet lines are separated by $\sim (1 + z_{\text{abs}}) \times 800 \text{ \AA}$ from the S II triplet; thus, at the redshifts $z_{\text{abs}} = 2 - 3$ of most DLAs, the two sets of spectral features fall in widely separated regions of the optical spectrum which may not be covered simultaneously by some instruments. For this reason, most measurements of the $[\text{S}/\text{Zn}]$ ratio in DLAs have become available only recently thanks to the wide spectral coverage and high ef-

Table 6. Interstellar sulphur and zinc measurements in damped Ly α systems.

QSO	z_{abs}	$\log N(\text{H I})$ (cm^{-2})	$\log N(\text{S II})$ (cm^{-2})	$\log N(\text{Zn II})$ (cm^{-2})	$[\text{Zn}/\text{H}]^a$	$[\text{S}/\text{Zn}]^b$	Ref. ^c
Q0000–2620	3.3901	21.41 ± 0.08	14.70 ± 0.03	12.01 ± 0.05	–2.07	+0.16	1, 2
Q0013–004	1.97296	20.83 ± 0.05	15.28 ± 0.03	12.74 ± 0.04	–0.76	+0.01	3
Q0100+130	2.3090	21.40 ± 0.05	15.13 ± 0.05	12.45 ± 0.10	–1.62	+0.15	2, 4
Q0407–4410	2.5505	21.13 ± 0.10	14.82 ± 0.06	12.44 ± 0.05	–1.36	–0.15	5
Q0407–4410	2.5950	21.09 ± 0.10	15.19 ± 0.05	12.68 ± 0.02	–1.08	–0.02	5
Q0551–366	1.96221	20.50 ± 0.08	15.38 ± 0.11	13.02 ± 0.05	–0.15	–0.17	6
0841+1256	2.3745	21.00 ± 0.10	14.77 ± 0.03	12.20 ± 0.05	–1.47	+0.04	7
HE2243–6031	2.33000	20.67 ± 0.02	14.88 ± 0.01	12.22 ± 0.03	–1.12	+0.13	8
B2314–409	1.8573	20.90 ± 0.10	15.10 ± 0.05	12.52 ± 0.03	–1.05	+0.05	9
Q2343+125	2.4313	20.35 ± 0.05	14.71 ± 0.08	12.45 ± 0.06	–0.57	–0.27	3, 10

^a $[\log (\text{Zn}/\text{H})_{\text{DLA}} - \log (\text{Zn}/\text{H})_{\odot}]$, where $\log (\text{Zn}/\text{H})_{\odot} = -7.33$ (Grevesse & Sauval 1998).

^b $[\log (\text{S}/\text{Zn})_{\text{DLA}} - \log (\text{S}/\text{Zn})_{\odot}]$, where $\log (\text{S}/\text{Zn})_{\odot} = 2.53$ (Grevesse & Sauval 1998).

^c References—1: Molaro et al. (2000); 2: Lu, Sargent, & Barlow (1998); 3: Petitjean, Srianand & Ledoux (2002); 4: Prochaska et al. (2001); 5: Lopez & Ellison (2003); 6: Ledoux, Srianand, & Petitjean (2002); 7: Centurion et al. (2003); 8: Lopez et al. (2002); 9: Ellison & Lopez (2001); 10: Dessauges-Zavadsky, Prochaska, & D’Odorico (2002).

iciency at blue and red wavelengths of the VLT/UVES combination.

In Table 6 we have collated from the literature all measurements of $[\text{S}/\text{Zn}]$ in DLAs from spectra obtained with 8–10 m class telescopes; references to the original works are given in the last column of the Table. The total sample consists of ten DLAs at redshifts $z_{\text{abs}} = 1.86 - 3.39$; their values of $[\text{S}/\text{Zn}]$ vs. $[\text{Zn}/\text{H}]$ are compared with the stellar measurements in Fig. 9. The behaviour of the $[\text{S}/\text{Zn}]$ ratio in DLAs is evidently not the same as that seen in Galactic stars. Taken together, the ten DLAs considered here do not show evidence for an α -element enhancement; the mean and standard deviation for the sample are $[\text{S}/\text{Zn}] = -0.01 \pm 0.15$. Considering only the seven DLAs with $[\text{Zn}/\text{H}] < -1$, we find $[\text{S}/\text{Zn}] = +0.05 \pm 0.11$.

It is hard to identify systematic effects which may be the cause of this apparent offset between DLAs and Galactic halo stars. The column density errors listed in Table 6, which in turn translate to the typical abundance errors illustrated in Fig. 9, are those quoted by the authors of the original papers, as referenced in the Table. These errors are the 1σ uncertainties returned by the absorption line fitting computer codes and generally reflect the random errors in the line equivalent widths. They are probably underestimates of the true uncertainties (see, for example, the discussion of this point by Kirkman et al. 2003), but this should result in an increased scatter of the data points in Fig. 9, rather than a systematic offset. Generally, the S II triplet lines are stronger than the Zn II doublet, so that saturation may be an issue. However, with three absorption lines available, it is normally possible to assess the degree of saturation reliably, unless the distribution of absorber properties is markedly irregular (Jenkins 1986); the line fitting programs used in the original analyses of the data in Table 6 are well up to this task. Similar considera-

tions apply to resolving the Zn II $\lambda\lambda 2026.1, 2062.7$ doublet lines from the nearby Mg I $\lambda 2026.5$ and Cr II $\lambda 2062.2$ lines.

Turning from ion column densities to element abundances, it is also difficult to find reasons why the abundance of S should have been systematically underestimated, or that of Zn overestimated. Both S II and Zn II are the major ionization stages of their respective elements in H I regions, and corrections for unobserved ion stages are expected to be unimportant (e.g. Vladilo et al. 2001). Neither S nor Zn show much affinity for dust and the problem is further lessened in DLAs which generally show only mild depletions of even the refractory elements (Pettini et al. 1997). Errors in the solar abundance scale do not seem a plausible explanation for the difference either. Recall that while the stellar abundances are derived differentially relative to the Sun, those in DLAs have to be referred to a solar scale; here we have adopted the meteoritic abundances of S and Zn from the compilation by Grevesse & Sauval (1998). However, as discussed earlier (Sect. 4.2 and 4.3), the S I lines used in the present study give a solar photospheric abundance of S which is the same as the meteoritic one, and while for Zn there is a 0.10 dex offset, this offset is in the wrong direction for reconciling stellar and DLA data.

In summary, on the basis of our current knowledge of S and Zn in the local interstellar medium, the values given in Table 6 should reflect the true interstellar abundances of these two elements in the high redshift galaxies giving rise to the damped Ly α systems. Thus, we are led to conclude that the difference between Milky Way stars and DLAs is probably real, confirming the earlier analysis by Centurion et al. (2000) which was based on noisier 4-m data. A similar conclusion has also been reached by several studies which targeted depleted elements (chiefly Si and Fe) and then attempted to correct for the fractions in

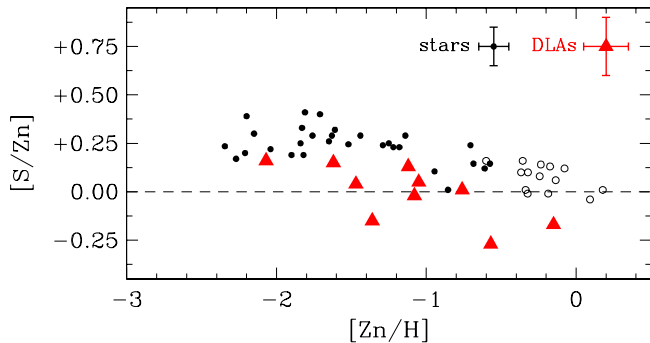


Fig. 9. $[S/Zn]$ vs. $[Zn/H]$ in Milky Way stars and damped Ly α systems. Typical errors are shown.

dust (e.g. Vladilo 2002 and references therein), although the method used here is clearly more direct, as it does not rely on the accuracy of the dust corrections.

Interpreted within standard chemical evolution models (e.g. Calura, Matteucci, & Vladilo 2003), the lack of α -element enhancement in DLAs may be taken as evidence for low and intermittent rates of star formation over their past history (relative to the time when we observe them). Put simply, in this scenario the overall metallicity grows only slowly with time and the iron-peak elements released by Type Ia supernovae can ‘catch-up’ with the overall chemical enrichment during quiescent periods between isolated bursts of star formation. Such a mode of star formation is seen locally in dwarf irregular and dwarf spheroidal galaxies whose stars also do not show an α -element enhancement at low metallicities (Carigi, Hernandez, & Gilmore 2002; Venn et al. 2003; Shetrone et al. 2003; Tolstoy et al. 2003), and is indeed envisaged in theoretical models of DLA galaxies (e.g. Mo, Mao, & White 1998).

Nevertheless, it is somewhat remarkable that we have not found even a single DLA with a high $[S/Zn]$ ratio in our (albeit small) sample. At lower redshifts ($z < 1$), DLA galaxies are a heterogeneous group, exhibiting a variety of morphologies and surface brightnesses (Boissier, Péroux, & Pettini 2003); if this is also the case at high z , we may have expected a wider range of $[S/Zn]$ values. Possibly the issue is still clouded by small number statistics, or there may be more fundamental differences between high- and low-redshift DLAs. The findings by Kanekar & Chengalur (2003) may be relevant here. These authors derived estimates of the spin temperature T_s in 24 DLAs, 11 of which (all at $z_{\text{abs}} < 1$) have optical identifications. Kanekar & Chengalur (2003) find that all DLAs with high values of spin temperature ($T_s \gtrsim 1000$ K) are identified with dwarf or low surface brightness galaxies, while DLAs with low values of T_s are invariably associated with large, luminous galaxies. Furthermore, low z DLAs exhibit both high and low values of T_s , while high redshift ($z_{\text{abs}} \gtrsim 2$) DLAs have preferentially high spin temperatures. The lack of a significant α -element enhancement in the DLAs considered

here can be understood within the picture put forward by Kanekar & Chengalur (2003), if dwarf and low surface brightness galaxies dominate the cross-section for DLA absorption at high redshift, and if these types of galaxies generally tend to have low and intermittent rates of star formation.

Centurión et al. (2000) and Vladilo (2002) suggested that there may be a mild trend of decreasing $[S/Zn]$ (and more generally $[\alpha/Fe]$) with increasing metallicity in DLAs. While the DLA data shown in Fig. 9 are not inconsistent with such a possibility, the number of reliable S and Zn abundance measurements needs to be considerably larger than the current sample before the reality of such a trend can be assessed statistically.

6. Summary and conclusions

One of the motivations for carrying out the present survey of S and Zn abundances in Galactic stars is the important role played by these two elements in deciphering the chemical enrichment and star formation histories of damped Ly α systems. Up to now measurements of the sulphur abundance in Galactic stars have been sparse and doubts have been raised as to whether S is a typical α -capture element formed in Type II supernovae (Israelian & Rebolo 2001; Takada-Hidai et al. 2002). The lack of data for sulphur, coupled with insufficient knowledge of the nucleosynthetic channels for the production of Zn, has led some (e.g. Prochaska et al. 2000) to question the validity of using these elements, and in particular their ratio, in the interpretation of the abundance patterns seen in DLAs.

The new data presented here have clarified the situation as regards Milky Way stars. By targeting the S I $\lambda\lambda 9212.9, 9228.1, 9237.5$ triplet we have overcome the limitations of most earlier studies and probed the abundance of sulphur with higher precision and to lower metallicities than had been possible previously. We find that the trend of $[S/Fe]$ as a function of $[Fe/H]$ is very similar to those of other typical α -capture elements, Mg, Si and Ca. $[S/Fe]$ is nearly constant at a level of $[S/Fe] \simeq +0.3$ dex in the metallicity range $-3.2 < [Fe/H] < -1.2$, starts to decrease at $[Fe/H] \simeq -0.7$, and reaches a solar ratio at $[Fe/H] \sim 0$. In the halo-disk transition region, at metallicities $-1.2 < [Fe/H] < -0.7$, there is significant scatter in the values of $[S/Fe]$. More stars in this interval should be studied to look for possible correlations between stellar kinematics and $[S/Fe]$. Precise abundance analyses by Fuhrmann (1998); Gratton et al. (2000); and Feltzing et al. (2003) have shown a clear separation in $[Mg/Fe]$ between thin and thick disk stars and it will be important to establish if this is also the case for $[S/Fe]$.

As far as zinc is concerned, we confirm the results of several earlier surveys which have shown that, to a first approximation, Zn tracks Fe over three orders of magnitude in $[Fe/H]$. There is some evidence for a small overabundance of Zn ($[Zn/Fe] \simeq +0.10$) for metal-poor disk stars and halo stars with $[Fe/H] < -2$. However, there may be

systematic errors in $[Zn/Fe]$ at a level of ± 0.1 dex due to the difficulty in analyzing the $\lambda\lambda 4722.2, 4810.5$ Zn I lines in the solar spectrum. Non-LTE effects on the derived zinc abundances are also a potential problem that should be addressed. New studies of the nucleosynthesis of zinc in supernovae and by the s -process in AGB stars would help in understanding the reasons why Zn behaves like an Fe-peak element and the origin of the 0.1 dex offset at low metallicities.

When we turn to damped Ly α systems, however, the Galactic pattern of S and Zn abundances does not seem to apply. The sample is still small (accurate measurements of $[S/Zn]$ are available for only ten DLAs) and there is scatter in the data but, taken at face value, there is no obvious α -element enhancement in DLAs. We can not identify any systematic effect in the data nor in their analysis which would mask such an enhancement, if it were there, and conclude that its absence is probably real. Presumably, it is indicative of a bursting history of star formation in the galaxies giving rise to damped systems. However, it is important to realise that a variety of recent observations suggest that the α -enhancement exhibited by metal-poor stars of the Milky Way may in fact be the exception rather than the rule—it is generally not seen in dwarf spheroidal and dwarf irregular galaxies (Venn et al. 2003; Shetrone et al. 2003; Tolstoy et al. 2003; Aloisi et al. 2003), in old stars of the Large Magellanic Cloud (Hill et al. 2000), in DLAs (this paper), in some Galactic halo stars with large orbits (Nissen & Schuster 1997), and in the globular cluster Pal 12 which may originally have been part of the Sgr dSph galaxy (Cohen 2003). The challenge now is to incorporate this rapidly growing set of abundance measurements into a comprehensive picture of the chemical evolution of galaxies.

Acknowledgements. The ESO staff at Paranal is thanked for carrying out the VLT/UVES service observations in a very competent way. In particular we acknowledge important advice on the observing procedure from Vanessa Hill and Francesca Primas. PEN acknowledges support from the Danish Natural Science Research Council (grant 21-01-0523). MA has been supported by grants from the Swedish Natural Science Research Council (grants F990/1999 and R521-880/2000), the Swedish Royal Academy of Sciences, the Göran Gustafsson Foundation and the Australian Research Council (grant DP0342613). This research has made use of the SIMBAD database, operated at CDS, Strasbourg, France.

References

- Aloisi, A., Savaglio, S., Heckman, et al. 2003, ApJ, 595, 760
 Alonso, A., Arribas, S., & Martínez-Roger, C. 1994, A&AS, 107, 365
 Alonso, A., Arribas, S., & Martínez-Roger, C. 1995, A&A, 297, 197
 Alonso, A., Arribas, S., & Martínez-Roger, C. 1996, A&A, 313, 873
 Asplund, M., Carlsson, M., Botnen, A.V. 2003, A&A, 399, L31
 Asplund, M., García Pérez, A.E. 2001, A&A, 372, 601
 Asplund, M., Gustafsson, B., Kiselman, D., & Eriksson, K. 1997, A&A 318, 521
 Asplund, M., Nordlund, Å., Trampedach, R., Stein, R.F. 1999, A&A, 346, L17
 Biémont, E., & Godefroid, M. 1980, A&A 84, 361
 Boissier, S., Péroux, C., & Pettini, M. 2003, MNRAS, 338, 131
 Calura, F., Matteucci, F., & Vladilo, G. 2003, MNRAS, 340, 59
 Carretta, E., Gratton, R., Cohen, J.G., Beers, T.C., & Christlieb, N. 2002, AJ, 124, 481
 Carigi, L., Hernandez, X., & Gilmore, G. 2002, MNRAS, 334, 117
 Carney, B.W. 1983, AJ 88, 610
 Carpenter, J.M. 2001, AJ, 121, 2851
 Centurión, M., Bonifacio, P., Molaro, P., Vladilo, G. 2000, ApJ, 536, 540
 Centurión, M., Molaro, P., Vladilo, G., et al. 2003, A&A, 403, 55
 Chen, Y.Q., Nissen, P.E., Zhao, G., Asplund, M. 2002, A&A, 390, 225
 Chen, Y.Q., Nissen, P.E., & Zhao, G. 2003, (in preparation)
 Chiappini, C., Matteucci, F., Beers, T.C., Nomoto, K. 1999, ApJ, 515, 226
 Cohen, J.G., 2003, submitted to AJ (astro-ph/0311187)
 Cutri, R.M., Skrutskie, M.F., Van Dyk, S., et al. 2003, Explanatory Supplement to the 2MASS All Sky Data Release, (IPAC/California Institute of Technology; <http://www.ipac.caltech.edu/2mass>)
 Dekker, H., D’Odorico, S., Kaufer, A., Delabre, B., & Kotzlowski, H. 2000, Proc. SPIE 4008, 534
 Dekker, H., Nissen, P.E., Kaufer, A., Primas, F., D’Odorico, S., Hanuschik, R.W. 2002, Proc. SPIE 4828, 139
 Dessauges-Zavadsky, M., Prochaska, J. X., & D’Odorico, S. 2002, A&A, 391, 801
 Ellison, S. L. & Lopez, S. 2001, A&A, 380, 117
 ESA 1997, The Hipparcos and Tycho Catalogues, ESA SP-1200
 Feltzing, S., Bensby, T., & Lundström, I. 2003, A&A, 397, L1
 François, P. 1987, A&A, 176, 294
 François, P. 1988, A&A, 195, 226
 Fuhrmann, K. 1998, A&A, 338, 161
 Goswami, A., Prantzos, N. 2000, A&A, 359, 191
 Gratton, R.G., Carretta, E., Desidera, S. et al. 2003, A&A, 406, 131
 Gratton, R., Carretta, E., Matteucci, F., & Sneden, C. 2000, A&A, 358, 671
 Grevesse, N., & Sauval, A.J. 1998, Space Science Reviews 85, 161
 Hill, V., François, P., Spite, M., Primas, F., & Spite, F. 2000, A&A, 364, L19
 Holweger, H., Müller, E.A. 1974, Solar Phys., 39, 19
 Israelian, G., Rebolo, R. 2001, ApJ, 557, L43
 Jenkins, E. B. 1986, ApJ, 304, 739
 Kanekar, N. & Chengalur, J. N. 2003, A&A, 399, 857
 Kirkman, D., Tytler, D., Suzuki, N., O’Meara, J. M., & Lubin, D. 2003, ApJS, in press (astro-ph/0302006)
 Kiselman, D. 1997, ApJ, 489, L107
 Kiselman, D., Nordlund, Å., 1995, A&A 302, 578
 Kurucz, R.L., Furenlid, I., Brault, J., & Testerman, L. 1984, Solar Flux Atlas from 296 to 1300 nm, National Solar Observatory, Sunspot, New Mexico
 Lambert, D.L., Luck, R.E. 1978, MNRAS, 183, 79
 Ledoux, C., Srianand, R., & Petitjean, P. 2002, A&A, 392, 781
 Lopez, S. & Ellison, S. L. 2003, A&A, 403, 573

- Lopez, S., Reimers, D., D'Odorico, S., & Prochaska, J. X. 2002, *A&A*, 385, 778
- Lu, L., Sargent, W. L. W., & Barlow, T. A. 1998, *AJ*, 115, 55
- Matteucci, F., Raiteri, C.M., Busso, M., Gallino, R., Gratton, R. 1993, *A&A*, 272, 421
- Mishenina, T.V., Kovtyukh, V.V., Soubiran, C., Travaglio, C., Busso, M. 2002, *A&A*, 396, 189
- Mitchell, W.E., & Mohler, O.C. 1965, *ApJ*, 141, 1126
- Mo, H. J., Mao, S., & White, S. D. M. 1998, *MNRAS*, 295, 319
- Molaro, P., Bonifacio, P., Centurión, M., et al. 2000, *ApJ*, 541, 54
- Nakamura T., Umeda H., Iwamoto K.I. et al. 2001, *ApJ*, 555, 880
- Nissen, P.E. 1994, *Rev. Mex. Astron. Astrofis.* 29, 129
- Nissen, P.E. 2003, *Carnegie Observatories Astrophysics Series*, vol. 4: Origin and Evolution of the Elements, ed. A. McWilliam & M. Rauch, (Cambridge: Cambridge Univ. Press), in press (astro-ph/0310326)
- Nissen, P.E., Primas, F., Asplund, M., & Lambert, D.L. 2002, *A&A*, 390, 235
- Nissen, P.E., & Schuster, W.J. 1997, *A&A*, 326, 751
- Norris, J.E, Ryan, S.G., & Beers, T.C. 2001, *ApJ*, 561, 1034
- Petitjean, P., Srianand, R., & Ledoux, C. 2002, *MNRAS*, 332, 383
- Pettini, M., Boksenberg, A., & Hunstead, R.W. 1990, *ApJ*, 348, 48
- Pettini, M., Ellison, S.L., Steidel, C.C., & Bowen, D.V. 1999, *ApJ*, 510, 576
- Pettini, M., King, D. L., Smith, L. J., & Hunstead, R. W. 1997, *ApJ*, 478, 536
- Prochaska, J. X., Wolfe, A.M., Tytler, D. et al. 2001, *ApJS*, 137, 21
- Prochaska, J. X., Naumov, S.O., Carney, B.W., McWilliam, A., Wolfe, A.M. 2000, *AJ*, 120, 2513
- Prochaska, J. X., Wolfe, A.M. 2002, *ApJ*, 566, 68
- Ryan, S.G., Norris, J.E., Beers, T.C. 1999, *ApJ*, 523, 654
- Savage, B.D., & Mathis, J.S. 1979, *ARA&A* 17, 73
- Schuster, W.J., Moitinho, A., Parrao, L., & Covarrubias, E. 2003, in preparation
- Schuster, W.J., & Nissen, P.E. 1988, *A&AS* 73, 225
- Schuster, W.J., & Nissen, P.E. 1989, *A&A* 221, 65
- Seaton, M.J., 1990, *J. Phys. B*, 23, 3255
- Shetrone, M., Venn, K.A., Tolstoy, E., Primas, F., Hill, V., & Kaufer, A. 2003, *AJ*, 125, 684
- Shchukina, N., Bueno, J.T. 2001, *ApJ*, 550, 970
- Snedden, C., Gratton, R.G., Crocker, D.A. 1991, *A&A*, 246, 354
- Stephens, A., & Boesgaard, A.M. 2002, *AJ*, 123, 1647
- Takada-Hidai, M., Takeda, Y., Sato, S., et al. 2002, *ApJ*, 573, 584
- Thévenin, F., & Idiart, T. 1999, *ApJ* 521, 753
- Tolstoy, E., Venn, K.A., Shetrone, M., Primas, F., Hill, V., Kaufer, A., & Szeifert, T. 2003, *AJ*, 125, 707
- Unsöld, A. 1955, *Physik der Sternatmosphären*, Springer Verlag, Berlin
- Uitenbroek, H. 1998, *ApJ*, 498, 427
- VandenBerg, D.A., Swenson, F.J., Rogers, F.J., Iglesias, C.A., & Alexander, D.R. 2000, *ApJ*, 532, 430
- Venn, K., Tolstoy, E., Kaufer, A., & Kudritzki, R. P. 2003, *Carnegie Obs. Astroph. Series*, Vol. 4, Origin and Evolution of the Elements, eds. A. McWilliam, & M. Rauch, in press (astro-ph/0305188)
- Vladilo, G. 2002, *A&A*, 391, 407
- Vladilo, G., Centurión, M., Bonifacio, P., & Howk, J. C. 2001, *ApJ*, 557, 1007